AD-A160 582 DISPERSION CHARACTERISTICS OF A DIELECTRIC LOADED 1/1
WAVEGUIDE(U) NAVAL SURFACE WEAPONS CENTER SILVER SPRING
MD H CROSBY ET AL. 30 JUL 84 NSWC/TR-84-338

UNCLASSIFIED F/G 9/1 NL

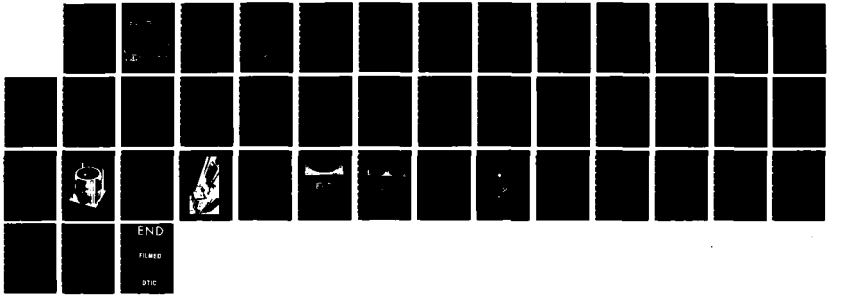

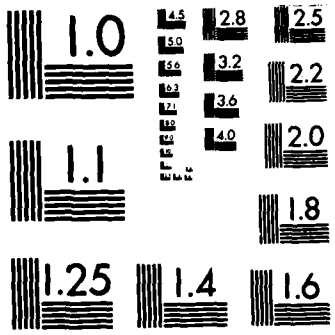

NSWC TR 84-338

(12)

AD-A160 582

DISPERSION CHARACTERISTICS OF A DIELECTRIC LOADED WAVEGUIDE

BY H. CROSBY J. CHOE Y. SONG A. KRALL

RESEARCH AND TECHNOLOGY DEPARTMENT

30 JULY 1984

NAVAL SURFACE WEAPONS CENTER

Dahlgren, Virginia 22448 • Silver Spring, Maryland 20910

REPORT DOCUMENTATION PAGE	READ INSTRUCTIONS BEFORE COMPLETING FORM
1. REPORT NUMBER: NSWC TR 84-338	2. GOVT ACCESSION NO.: AD-A160 582
	3. RECIPIENT'S CATALOG NUMBER
4. TITLE (and Subtitle): DISPERSION CHARACTERISTICS OF A DIELECTRIC LOADED WAVEGUIDE	5. TYPE OF REPORT & PERIOD COVERED
	6. PERFORMING ORG. REPORT NUMBER
7. AUTHOR(s): H. Crosby, J. Choe, Y. Song, and A. Krall	8. CONTRACT OR GRANT NUMBER(s)
9. PERFORMING ORGANIZATION NAME AND ADDRESS: Naval Surface Weapons Center (Code R43), 10901 New Hampshire Avenue, Silver Spring, MD 20903-5000	10. PROGRAM ELEMENT, PROJECT, TASK AREA & WORK UNIT NUMBERS
11. CONTROLLING OFFICE NAME AND ADDRESS	12. REPORT DATE: 30 July 1984
	13. NUMBER OF PAGES: 44
14. MONITORING AGENCY NAME & ADDRESS (if different from Controlling Office)	15. SECURITY CLASS. (of this report): UNCLASSIFIED
	15a. DECLASSIFICATION/DOWNGRADING SCHEDULE

16. DISTRIBUTION STATEMENT (of this Report)
Approved for public release; distribution is unlimited

17. DISTRIBUTION STATEMENT (of the abstract entered in Block 20, if different from Report)

18. SUPPLEMENTARY NOTES

19. KEY WORDS (Continue on reverse side if necessary and identify by block number)
Dielectric Loaded Waveguide
Resonant Cavity
Dispersion Curves
Mode Identification

20. ABSTRACT (Continue on reverse side if necessary and identify by block number)
The dispersion curves of the TE_{01} modes of dielectric clad waveguides were determined experimentally and compared with theory.

Waveguide impedance

DD FORM 1 JAN 73 1473 EDITION OF 1 NOV 68 IS OBSOLETE
S/N 0102-LF-014-6601

FOREWORD

We experimentally studied the dispersion characteristics of the dielectrically loaded waveguide, one of the slow wave structures that broadens the bandwidth of the gyrotron amplifier. The waveguide is composed of an aluminum cylinder. Within and concentric to this cylinder is a dielectric cylinder the outer radius of which is touching the metal cylinder.

The mode of interest is the azimuthally symmetric TE_{01} mode. The mode was studied by perturbing the field of a resonant cavity with the same cross section as the waveguide. From a large number of resonances the family of resonances belonging to the TE_{01n} cavity mode were identified (n is the axial mode number). Positive identification of the modes was based on determining the axial and aximuthal mode numbers. This was accomplished by noting the change in output power of the cavity as a small metal perturber was pulled along or rotated about the axis of the cavity.

The parameters that were experimentally varied were the thickness and dielectric constant of the dielectric cylinder.

Approved by:

H. R. RIEDL, Head
Radiation Division

CONTENTS

ILLUSTRATIONS

TABLES

SECTION 1

INTRODUCTION

The gyrotron is a vacuum tube capable of producing high (10 KW avg) power output in the millimeter and sub-millimeter wavelength region. Its recent application to millimeter wave radar and nuclear fusion could be greatly enhanced if wide instantaneous bandwidths were available. Choe and Uhm[1] indicate that wide instantaneous bandwidths are possible with various slow wave structures. This project investigates those slow wave structures to experimentally verify the predictions.

In a microwave tube such as a gyrotron the energy from an electron beam is converted to RF energy. Figure 1 shows a dispersion curve for an electron beam mode $\omega_B(k)$, and a dispersion curve for a vacuum waveguide mode, $\omega_G(k)$. The dispersion curve for an electron beam is given by

$$\omega_B = kV_z + \omega_c$$

$$\omega_c = \frac{eB_0}{mc}$$

where V_z is the velocity of the electron in the axial direction, ω_c is the cylotron frequency, e the charge on an electron, B_0 the D.C. magnetic field strength, m the electron mass, c the speed of light in a vacuum, and k the axial wavenumber. The dispersion curve for the vacuum waveguide is dependent on the internal slow wave structure. Energy conversion occurs only where the two dispersion curves ω_B and ω_G intersect. For the tube to be broadband the

shape of the ω_G curve can be altered so that $\omega_G \cong \omega_B$ over a broad range of frequencies. The reason ω_G, not ω_B, is changed is that it is much easier to change a slow wave structure in a waveguide than an electron gun or magnetic field structures that control the electron trajectory.

One purpose of these experiments is to investigate how the parameters of a slow wave structure affect the shape of the dispersion curve, ω_G. Specifically, in this experiment the dispersion characteristics of a dielectric loaded waveguide are investigated. Diagrams of this structure are shown in Figures 2 and 3. The parameters that were varied were the dielectric constant of the dielectric cylinder and the relative thickness of this cylinder measured by the ratio, R_w/R_c, defined later. The dielectric loaded waveguide was chosen as a first experiment because the theory of the structure is well known. Experimental results checked against this theory lend credibility to the experimental method of mode identification.

Experimentally, the resonant frequencies of a dielectric loaded cavity were measured. From a large number of possible resonances, a particular family of resonances belonging to a family of transverse electric modes, were identified. This family of resonant modes are commonly used in gyrotons. Positive identification of the modes was based on determining the azimuthal and axial mode numbers. By counting the number of nulls in the output energy of the cavity as a metallic probe was pulled along or rotated about the axis of the cavity, the axial and azimuthal mode numbers were determined respectively; the number of nulls being the mode number. Once the family of resonances had been identified, the dispersion characteristic was obtained by

plotting the resonant frequency of each family member against its corresponding axial cavity wavelength.

SECTION 2

THEORY

As illustrated in Figure 2, the system configuration consists of an annular dielectric cylinder of outside radius R_c and inside radius R_w, located inside and concentric with a cylindrical conducting waveguide of radius R_c. The dielectric cylinder is referred to as region 2, and the empty volume inside this cylinder is region 1. It is assumed that the waveguide walls are infinitely conducting, and the dielectric is lossless. Cylindrical coordinates, (r,Θ,z) are used in this analysis.

In the subsequent analysis, we adopt a normal mode approach in which all the components of the electromagnetic field are assumed to vary according to

$$\psi(\vec{x},t) = \phi(r)\exp\left[i(\ell\theta + kz - \omega t)\right] \tag{1}$$

where ω is the eigen frequency, k is the axial wave number, and ℓ is the azimuthal mode number.

Maxwell equations, in CGS units after Jackson,[2] for the electric and magnetic field amplitudes can be expressed as

$$\nabla \times \vec{E}(\vec{x}) = i(\omega/c)\ \vec{B}(\vec{x}),$$

$$\nabla \times \vec{B}(\vec{x}) = \left(\frac{4\pi}{c}\right)\ \vec{J}(\vec{x}) - i\mu\left(\frac{\omega}{c}\right)\vec{E}(\vec{x}), \tag{2}$$

where c is the speed of light in vacuo, $\vec{E}(\vec{x})$ and $\vec{B}(\vec{x})$ are the electric and magnetic fields respectively, and the electric current density, $\vec{J}(\vec{x})$, vanishes except at $r = R_c$.

At $r = R_c$ the boundary conditions require that the tangential electric field and the normal magnetic field must vanish at the surface of a conductor, i.e.,

$$\begin{aligned} E_\theta(r = R_c) &= 0, \\ E_z(r = R_c) &= 0, \\ B_r(r = R_c) &= 0. \end{aligned} \tag{3}$$

At $r = R_w$, the interface between the dielectric and air, the boundary conditions require that the tangential component of the electric and magnetic fields are continuous and the normal components of the electric displacement field, and the magnetic field are continuous, i.e.

$$\varepsilon_1 E_{r1}\ (r = R_w) = \varepsilon_2 E_{r2}(r = R_w), \qquad B_{r1}(r = R_w) = B_{r2}(r = R_w),$$

$$E_{\theta 1}(r = R_w) = E_{\theta\ 2}(r = R_w), \qquad B_{\theta 1}\ (r = R_w) = B_{\theta 1}\ (r = R_w), \tag{4}$$

$$E_{z1}(r = R_w) = E_{z2}\ (r = R_w), \qquad B_{z1}(r = R_w) = B_{z2}(r = R_w).$$

The number on the subscripts refer to region 1 or region 2.

From Maxwell's equations in cylindrical coordinates it can be shown that the differential equation for the axial components of the electric and magnetic fields are

$$\left(\frac{1}{r}\frac{\partial}{\partial r}\left(r\frac{\partial}{\partial r}\right) - \frac{\ell^2}{r^2} + \frac{\omega^2}{c^2} - k^2\right)\begin{Bmatrix} E_z(r) \\ H_z(r) \end{Bmatrix} = 0 \tag{5}$$

Matching E_z and H_z boundary condition at R_c and R_w we get solutions to Eq. (5),

$$E_z(r) = a \begin{cases} J_\ell(P_1 r), & 0 \leq r < R_w \\ \dfrac{J_\ell(R_c P_2) N_\ell(rP_2) - N_\ell(R_c P_2) J_\ell(rP_2)}{J_\ell(P_1 R_w)\left[N_\ell(R_w P_2) J_\ell(R_c P_2) - J_\ell(R_w P_2) N_\ell(R_c P_2)\right]}, & R_c \geq r \geq R_w \end{cases} \tag{6}$$

for the electric field, and

$$B_z(r) = b \begin{cases} J_\ell(P_1 r), & 0 \leq r \leq R_w \\ \dfrac{J'_\ell(R_c P_2) N_1(rP_2) - N'_\ell(R_c P_2) J_\ell(rP_2)}{J_\ell(P_1 R_w)\left[N_\ell(R_w P_2) J'_\ell(R_c P_2) - J_\ell(R_w P_2) N'_\ell(R_c P_2)\right]}, & R_c \geq r \geq R_w \end{cases} \tag{7}$$

for the magnetic field. In equations (6) and (7), a and b are constants, $J_\ell(x)$ and $N_\ell(x)$ are the Bessel functions of order ℓ of the first and second kinds respectively, the prime (') denotes differentiation of the Bessel functions with respect to x, and the parameter P is defined by

$$P_m = \sqrt{\varepsilon_m \omega^2/c^2 - k^2} \ .$$

Of the equations obtained by application of the remaining boundary conditions, those obtained by matching B_r and B_θ are one of two pairs that are linearly independent.

From Maxwell's equations (2) the azimuthal component of the magnetic field, B_θ , is expressed as

$$B_\theta = \frac{1}{p^2} \left[\frac{1}{r} \frac{\partial^2 B_z}{\partial \theta \partial z} + i\mu\varepsilon \frac{\omega}{c} \frac{\partial E_z}{\partial r} \right] , \tag{8}$$

and the radial component, B_r, is expressed as

$$B_r = \frac{1}{p^2} \left[\frac{\partial^2 B_z}{\partial r \partial z} - i\mu\varepsilon \frac{\omega}{c} \frac{1}{r} \frac{\partial E_z}{\partial \theta} \right], \tag{9}$$

Substituting equations (6) and (7) into equation (9) and substituting this result into the B_r boundary condition of equation (3) we can solve for the ratio of a and b. Next, substituting equation (6) and (7) into equation (8) and substituting that result into the B_θ boundary condition of equation (3) with the above result for the ratio of a and b, the following dispersion relation is obtained;

$$\left[\frac{\omega}{c} \frac{k}{R_w} \ell \left(\frac{\varepsilon_1 - \varepsilon_2}{P_1^2 P_2^2}\right) J_\ell(P_1 R_w)\right]^2 = D_E(\omega,k)\, D_M(\omega,k), \tag{10}$$

where D_E, the transverse electric dielecric function, is given by

$$D_E = \frac{J'_\ell(R_w P_1)}{P_1} - \frac{J_\ell(R_w P_1)}{P_2} \quad \frac{N'_\ell(R_c P_2)\, J'_\ell(R_c P_2) - N'_\ell(R_c P_2)\, J'_\ell(R_w P_2)}{N_\ell(R_w P_2)\, J'_\ell(R_c P_2) - N'_\ell(R_c P_2)\, J_\ell(R_w P_2)} \tag{11}$$

and D_M, the transverse magnetic dielectric function, is given by

$$D_M = \frac{\varepsilon_1}{P_1} J'_\ell(R_w P_1) - \frac{\varepsilon_2 J_\ell(R_w P_1)}{P_2} \frac{N'_\ell(R_w P_2) J_\ell(R_c P_2) - N_\ell(R_c P_2) J'_\ell(R_w P_2)}{N_\ell(R_w P_2) J_\ell(R_c P_2) - N_\ell(R_c P_2) J_\ell(R_w P_2)} \tag{12}$$

In general these modes are hybrid, but when the mode is azimuthally symmetric (i.e. $\ell = 0$), the modes are either transverse magnetic or transverse elecric. The modes of interest in this experiment are the TE_{01}, where the azimuthal mode number is 0 and, the radial mode number is 1. For $\ell = 0$ equation (10) becomes $D_M(\omega, k) D_E(\omega, k) = 0$. Two solutions to this equation are $D_M(\omega, k) = 0$ and $D_E(\omega, k) = 0$. We are interested in the transverse electric case $D_E(\omega, k) = 0$.

This is the dispersion relation for the TE_{01} mode. From equation (11) $D_E(k, \omega)$ for a given ω is symmetric in the axial wave number k [$D_E(-k, \omega) = D_E(k, \omega)$]. This means identical traveling waves propagating in the positive and negative axial direction exist. These waves when combined form standing waves. Standing waves can be produced by terminating the infinite waveguide with conducting plates and forming a cavity. For a cavity, equation (1) becomes

$$\psi = \phi(r) \exp i[(\ell\theta - \omega t)] \begin{matrix} \sin kz \\ \cos kz \end{matrix} \tag{13}$$

The axial number k becomes $n\,\pi/L$ where L is the axial length of the cavity and

The axial number k becomes n π/L where L is the axial length of the cavity and n is the axial mode number. The azimuthal and radial cavity mode patterns are the same as those of the waveguide; thus the cavity can be used to determine the waveguide dispersion characteristics. The cavity modes of interest are the TE_{01n} modes corresponding to the TE_{01} waveguide mode.

SECTION 3

EXPERIMENTS

The purpose of this experiment is to verify the theoretical dispersion relation derived in Section II for the dielectric clad cavity. The dispersion relation is an expression relating the frequency, ω , and the wave number, k. From this relation the phase velocity and group velocity of the wave can be measured. The phase velocity, $v_p = \omega/k$, and the group velocity, $v_g = d\omega/dk$

To experimentally determine the relation between ω and k those resonant frequencies belonging to the TE_{01} mode have to be identified, and the wavelength of those modes from which k can be determined has to be measured.

To determine the wavelength of a given mode the distance between successive peaks of the field in the axial direction of propagation has to be measured.

To identify the modes, in addition to axial characteristics of the field mentioned above, the azimuthal and radial characteristics of the field have to be measured. It is shown in Section 2 that if the dispersion relation is symmetric in k, $[\omega(k) = \omega(-k)]$ for a given ω, the azimuthal and radial field configuration will be unchanged by converting waveguide to cavity. The advantage of using a cavity over waveguide in measuring field configuration is

the standing wave in a cavity is spatially static and therefore much easier to measure than the traveling wave in the waveguide. Each cavity resonance will yield a standing wave mode that corresponds to one of the continuous waveguide modes. For a given waveguide mode the cavity has a resonant frequency at each value of the wave number, k, where $k = n \pi/L$. Each resonance is a discrete point on the continuous waveguide dispersion curve.

A. Experimental Apparatus

The experiment is centered around the dielectric clad cavity. A photograph of the cavity with one of the end plates removed is shown in Figure 3. Figure 4 is a diagram of the cavity cross section. The cavity is a hollow aluminum cylinder with an inside radius, R_c = 3". For reasons to be discussed in the next section, the length of the cavity was varied. Lengths of 2 inches, 4 inches, and 6 inches were used. Inside the aluminum cylinder is a concentric dielectric cylinder with an inner radius of R_w composed of pourable dielectric powder. The dielectric powder was held in place by a thin walled hollow styrofoam cylinder. This cylinder was carefully machined because it was found that slight variations in the magnitude of R_w affect field profile. A low density styrofoam, ε=1.029, was used because its dielectric constant is close to that of air making it transparent to the field. Two of the cavity parameters that affect the dispersion relation are the dielectric constant and the thickness of the dielectric cylinder. The dispersion curves were measured for cylinders with relative permittivity of 4.5 and 14. For each dielectric the cylinders had thicknesses where R_w/R_c = 0.9 and 0.8.

R_w/R_c is the ratio of the inner to the outer radius of the dielectric cylinder (See Figure 4).

The probe is a thin copper disk attached to a styrofoam wand. The wand is attached perpendicularly to a thin, 1/16" diameter, lucite rod. The rod lies along the axis of the cavity and exits both ends of the cavity through holes drilled in the end plates. With the rod the probe can be translated along or rotated about the axis of the cavity (see Figures 3 and 4).

Figure 5 is a photograph of the experimental apparatus and Figure 6 is a schematic of the apparatus. Microwave power is fed into the cavity by a sweep oscillator through an input coupler composed of a 1/8" diameter loop of wire that penetrates the cavity through one of the end plates. The output coupler is identical to the input coupler and enters the cavity through the opposite end plate. The couplers are located at a radial distance of 1.5 inches from the axis of the cylinder. The loops of the couplers lie in the same plane and are connected together so that they rotate simultaneously.

The output coupler is fed into a spectrum analyzer. The output power at a given input frequency to the cavity is proportional to the height of the peak on the spectrum analyzer. The vertical output of the spectrum analyzer is fed into the vertical input of a chart recorder. The lucite rod that carries the probe is connected to the carriage of the chart recorder with nylon thread. The other end of the lucite rod is attached to a counter weight with nylon thread. Starting the internal linear horizontal drive of the chart recorder pulls the probe through the cavity and records the changes in the

field due to the perturbation of the probe.

B. Mode Identification Method

Experimentally the resonant frequencies of a dielectrically loaded cavity were measured. From a large number of possible resonances a particular family of resonances belonging to the TE_{01n} modes, mostly used for the gyrotrons, were identified. For positive identification of these modes, it was sufficient to determine the azimuthal and axial mode numbers. The radial mode numbers were not necessary because the TE_{01n} and TE_{02n} modes are sufficiently far apart in frequency not to be confused.

The field configuration was identified by perturbing the cavity field with a small metal probe and observing the change in output power caused by the shift of the resonant frequency. Positions where the electric field is maximum are perturbed the most and can therefore be located with respect to zero electric field where perturbations are minimal. Variations in the electric field in both the axial and azimuthal direction were measured. To measure the axial variation of the field a resonance is first located. This is done by removing the effect of the probe by shorting it against an end plate. The sweep oscillator is tuned until a resonance peak is observed on the screen of the spectrum analyzer; the probe is then pulled along the cavity axis by the chart recorder carriage. As the probe is moved it disturbs the field by causing a slight change in the resonant frequency of the cavity. Since the oscillator is initially tuned to the maximum of the resonance, a shift in cavity resonance results in the oscillator being tuned

to other than a maximum. This is seen on the spectrum analyzer screen as a change in the height of the output power. The chart recorder records the relative variations in the field as the probe is pulled through the cavity. Thus, the chart recorder records a negative of the field configuration; areas of maximum chart recorder amplitude are regions of minimum field strength and vise versa.

To measure the azimuthal variation of the field the lucite rod that carries the probe is detached from the chart recorder carriage. Keeping the axial position fixed, the probe is turned about the axis of the cylinder while the chart recorder carriage is moving, recording the azimuthal variation in the field.

Counting the number of nulls on the recorder image as the probe is pulled along or rotated about the cavity axis, determines the axial and radial mode number respectively. Figures 7 and 8 show the chart recorder output for the TE_{011} and TE_{012} modes for a dielectric constant of 4.5 with the ratio $R_w/R_c = 0.9$.

C. Results

Obtaining a probe which has reasonably measurable effects on the field is a problem and usually requires a few trials before success is obtained. To illustrate this point, it can be seen from Figure 9, that the maximum field strength is in the dielectric. For a probe to make a measurable perturbation of the field it should be in the dielectric, as close to it as possible, or

large enough to intersect a significant portion of the electric field. In the first experiments the dielectric powder was held in a place with a solid styrofoam cylinder. A small metal needle lying parallel to the axis of the cavity was pulled through the dielectric powder. This probe had little measurable effect on the field because it didn't have enough surface parallel to the electric field. A probe with a larger crossectional area couldn't be pulled through the dielectric powder. The solution was the probe configuration and hollow styrofoam cylinder shown in Figure 3. The circular copper probe could made as large as needed and as close to the region of maximum field in the dielectric cylinder as necessary to get a measurable perturbation of the field.

Figure 10 shows the effects of probe diameter on the field configuration. The effect of the larger probe was to distort the field profile. Although the field was distorted by the probe, the azimuthal and axial symmetries on which mode identification was based were preserved. In fact some distortion enhanced the field picture by exaggerating the differences between regions of high and low fields.

To avoid too much distortion it was found that probe diameter should be small compared to the wavelength and therefore should decrease with increasing frequency. On the other hand, the probe should increase in diameter with increasing dielectric constant. With a large dielectric constant most of the electric field was confined to the dielectric cylinder; thus a large diameter probe was required to intersect enough electric field in region 1 to induce a detectable perturbation (see Figure 9).

Mode density is the limiting factor in identifying modes at high frequencies. Overlapping modes make identification difficult. It is well known that the number of modes in a cavity in a unit frequency interval increases with the square of the frequency and with the volume. Therefore, for a unit interval about a given frequency, the number of modes can be decreased by decreasing the volume of the cavity. The cavity volume in this experiment was decreased by decreasing the cavity length. Cavity lengths of 2 inches, 4 inches and 6 inches were used. As an example, from Table 1, consider the TE_{011} mode of a dielectric clad cavaity with $R_w/R_c = 0.9$ and $\varepsilon = 14.0$. This mode for a 6 inch cavity length resonates at 2285 MHz while the same mode for the 2 inch cavity resonates at 2912 MHz. Higher frequency points on the dispersion curve can be obtained using the shorter cavities.

Coupling energy into the cavity at higher frequencies and dielectric constants is also a problem. Referring to Figure 9, as frequency and/or dielectric constant was increased, the field concentrates in the dielectric. The couplers initially penetrated the end plates a radial distance of 1.5 inches from the axis of the cavity. For low frequencies and/or low dielectric constants the modes have enough electric field flux in region 1 for the probe to make a measurable perturbation on the field. This is not the case for high frequencies and/or high dielectric constants. To remedy this situation the couplers were placed so they penetrated the dielectric cylinder. Since this is the location of maximum field strength, maximum coupling with these modes was achieved, increasing the field strength in the region 1 of the cavity and allowing the probe to have a measurable effect on the output power.

Four experimental dispersion curves were produced. One for each combination of dielectric powder and cylinder thickness. Tables 1 and 2 show the data for these experiments. The data are plotted in Figures 11 and 12. The solid curves are the theoretical values while the points are the experimental results. The agreement between theory and experiment is considered good; within three percent for all the data.

Referring to the dispersion curves in Figures 11 and 12 the $\omega = ck$ is the dispersion relation for light in a vacuum, and the $\omega = ck/\sqrt{\varepsilon}$ is the dispersion relation for light in a dielectric medium of dielectric constant, ε. The area above the $\omega = cK$ curve is called the fast wave region because the phase velocity, ω/k, is greater than the speed of light. The area below this curve is the slow wave region. As frequency is increased, all the dispersion curves cross from the fast wave region into the slow wave region, and approach the $\omega = ck/\sqrt{\varepsilon}$ wave asymtopically. This is because the field concentrates in the dielectric as frequency and/or dielectric constant increase. At high enough frequencies almost all the field is in the dielectric cylinder, making the dielectric cylinder appear to the field as if were a continuous dielectric medium.

It can be seen from the data that as dielectric constant and/or dielectric cylinder thickness are increased, the curves cross into the slow wave region at lower frequencies and approach the $\omega = ck/\sqrt{\varepsilon}$ curve

asymptotically at a faster rate. The group velocity, $v_g = d\omega/dk$, , becomes nearly constant and its slope decreases. Thus by adjusting the parameters of dielectric constant and cylinder thickness the shape of the dispersion curve can be controlled.

SECTION 4

CONCLUSIONS

In this experiment selected properties of electromagnetic wave propagation in a dielectric loaded waveguide have been investigated. The dispersion relations for the waveguide were obtained by examining the resonances of a cavity with the same radial cross section as the waveguide. From a large number of resonances, those belonging to the TE_{01n} mode were identified. The dispersion relation of these modes was obtained by plotting the resonant frequency against the axial cavity wavelength.

The agreement between theory and experiment was considered good. The largest deviation between theory and experiment was three percent while most of the measurements were within one percent.

The close agreement between theory and experiment gives confidence that the method of mode identification used in this experiment can be used to measure the dispersion characteristics of other slow wave structures.

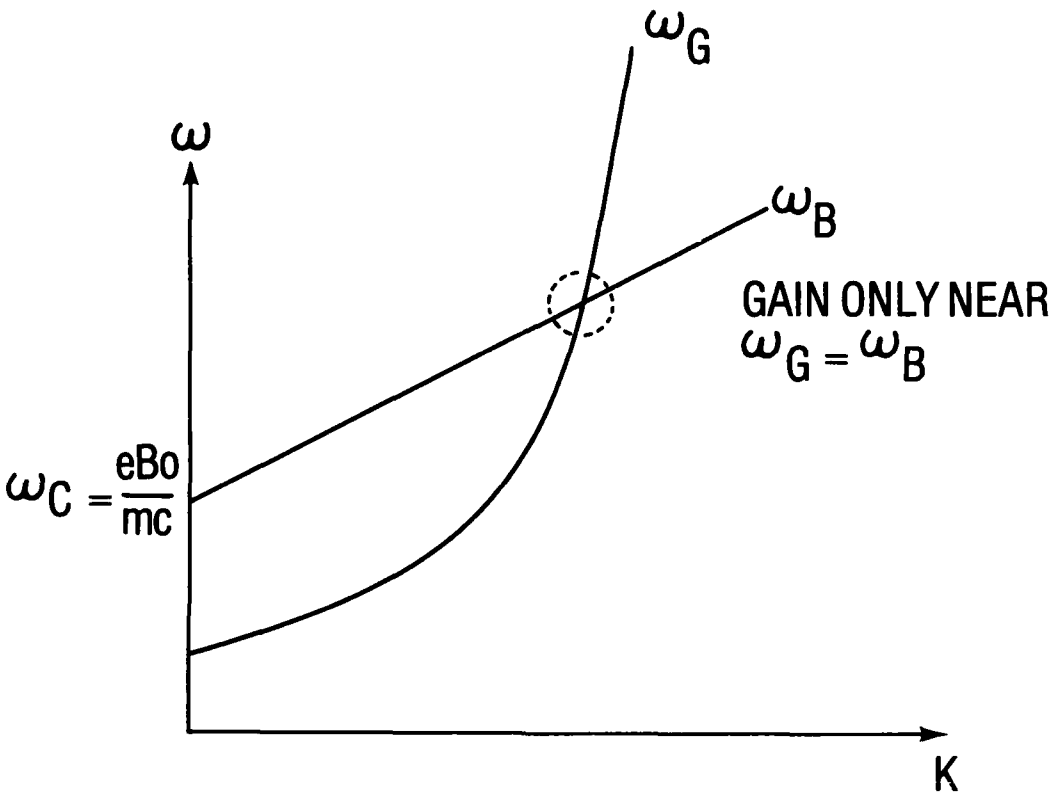

FIGURE 1. DISPERSION CURVES OF AN ELECTRON BEAM MODEL AND A SLOW WAVE STRUCTURE

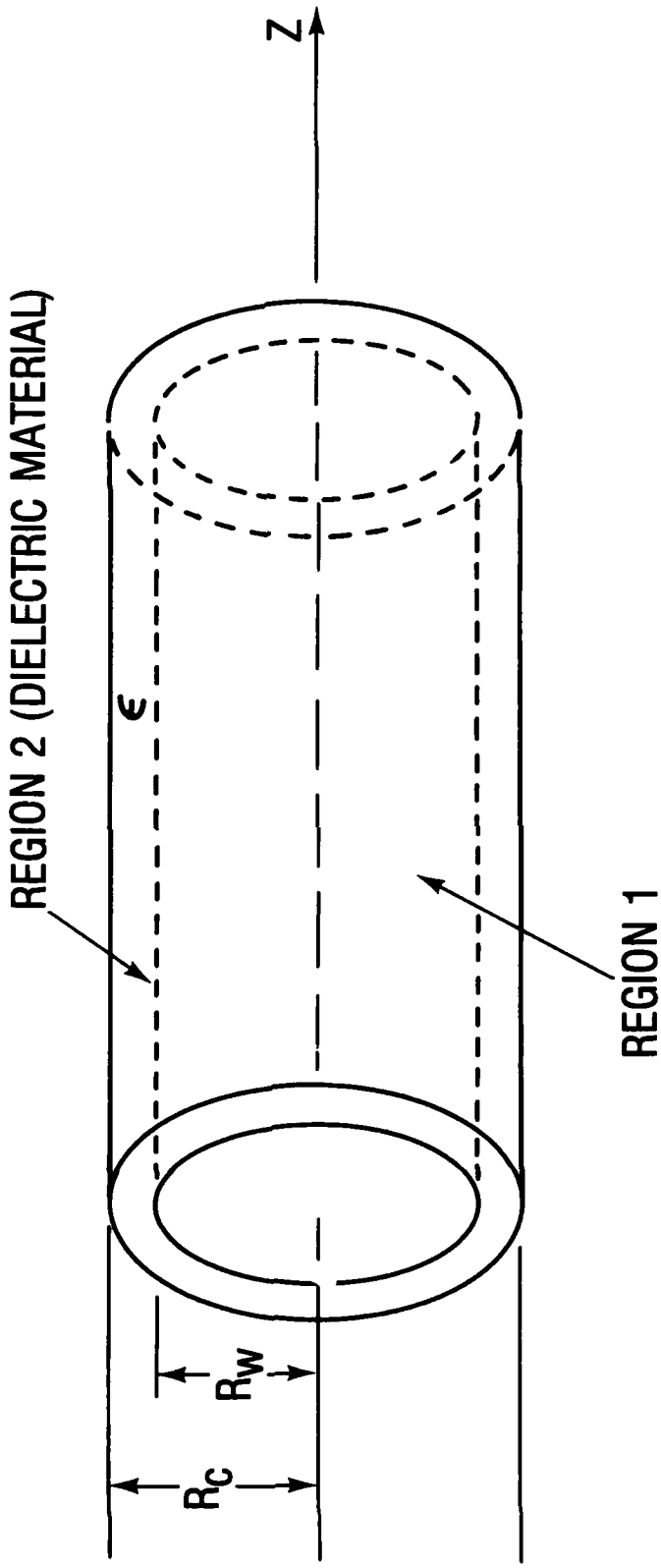

FIGURE 2. DIELECTRIC LOADED WAVEGUIDE

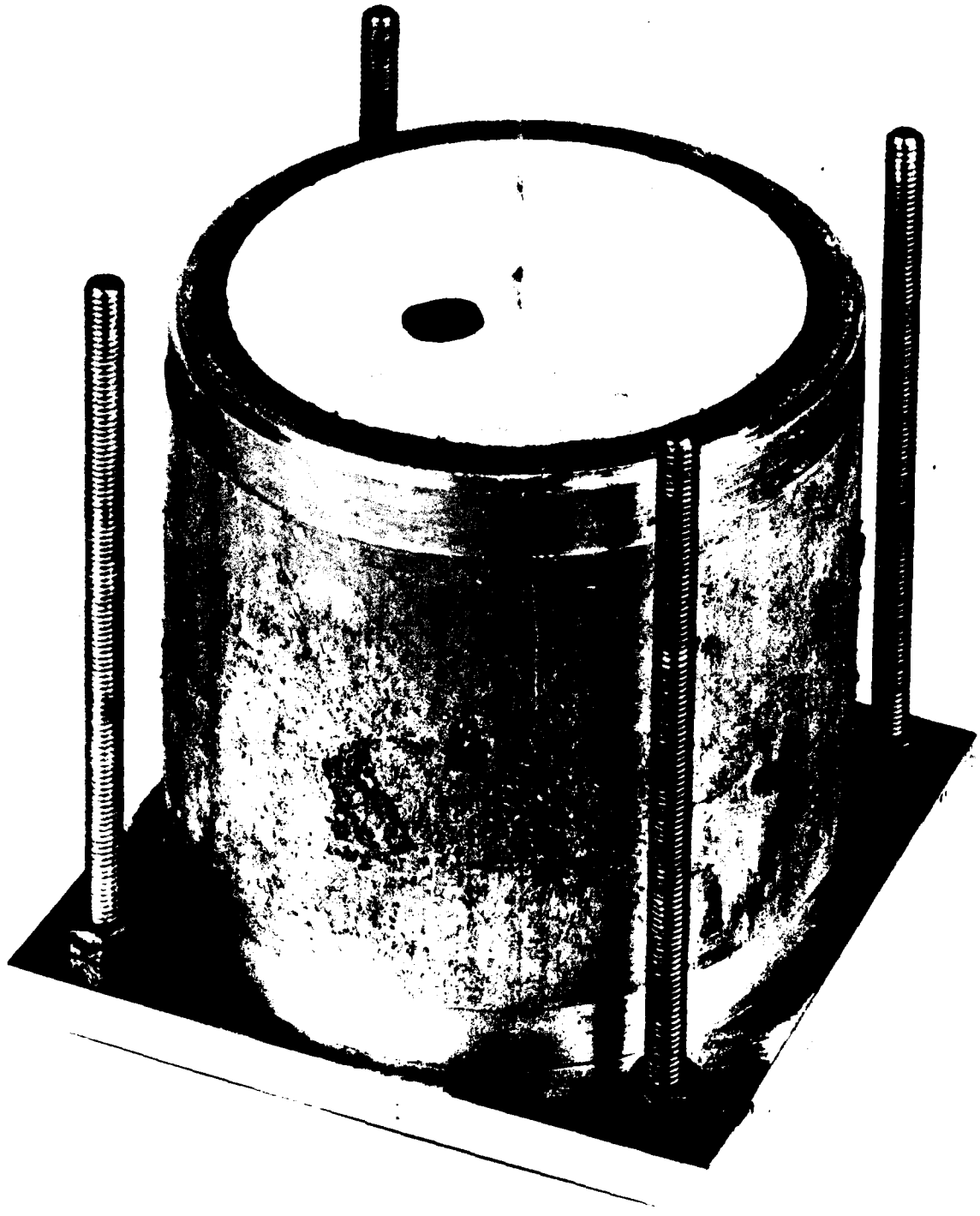

FIGURE 3. DIELECTRIC LOADED CYLINDRICAL CAVITY

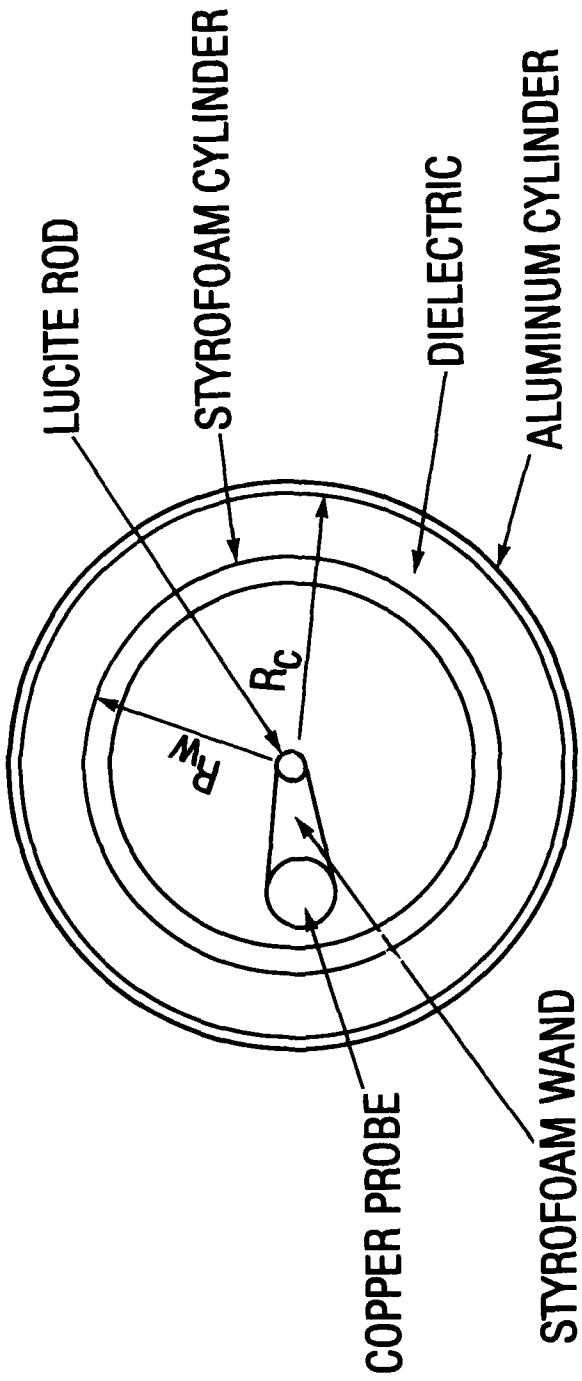

FIGURE 4. CROSS SECTION OF CAVITY

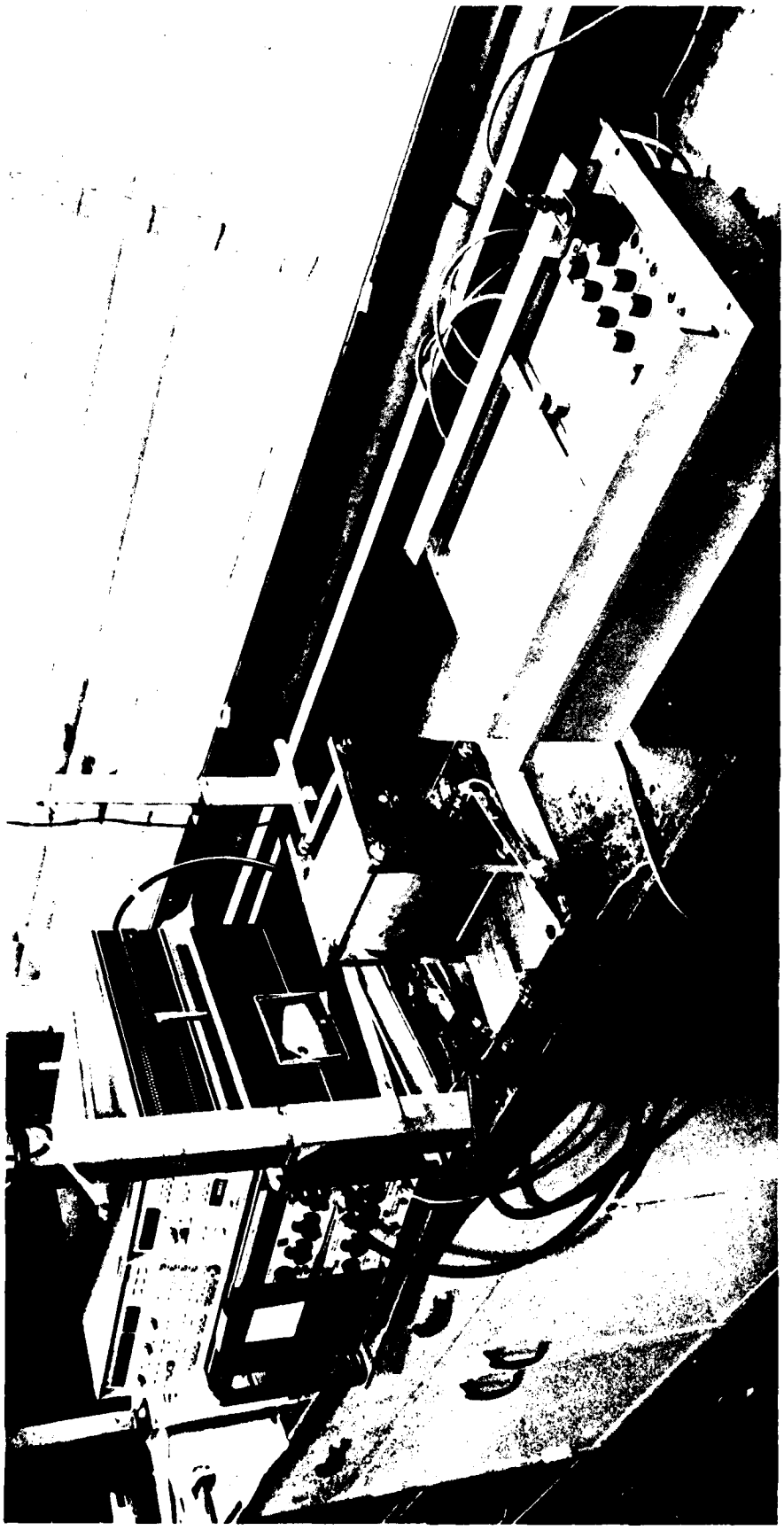

FIGURE 5. EXPERIMENTAL APPARATUS

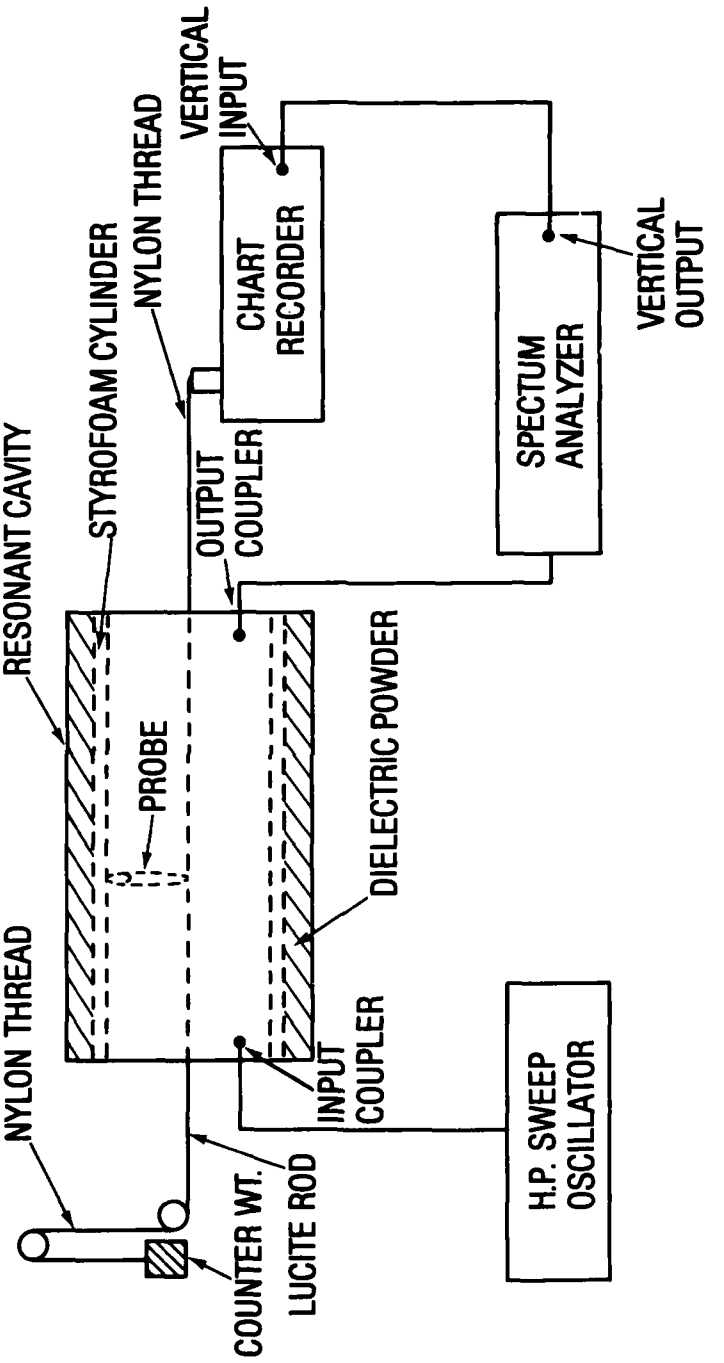

FIGURE 6. DIAGRAM OF EXPERIMENTAL APPARATUS

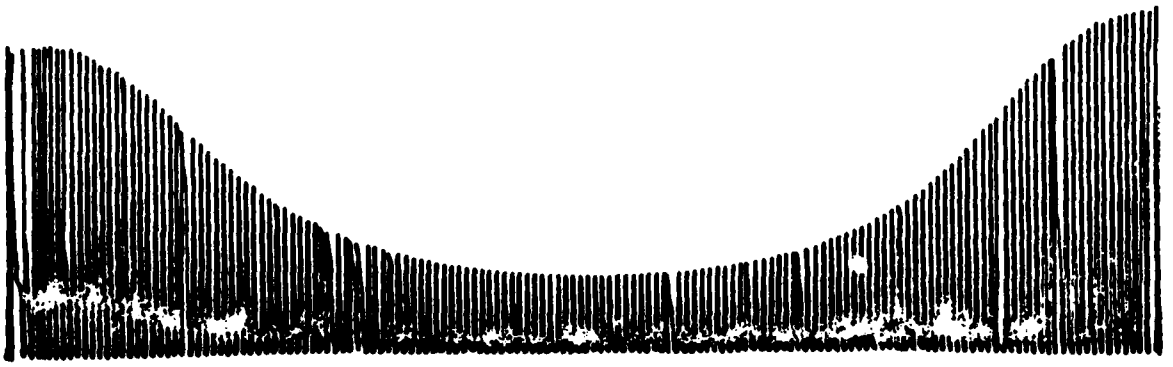

Z VARIATION

θ VARIATION

FIGURE 7. AXIAL AND AZIMUTHAL VARIATION OF TE_{011} MODE 2521 MHZ

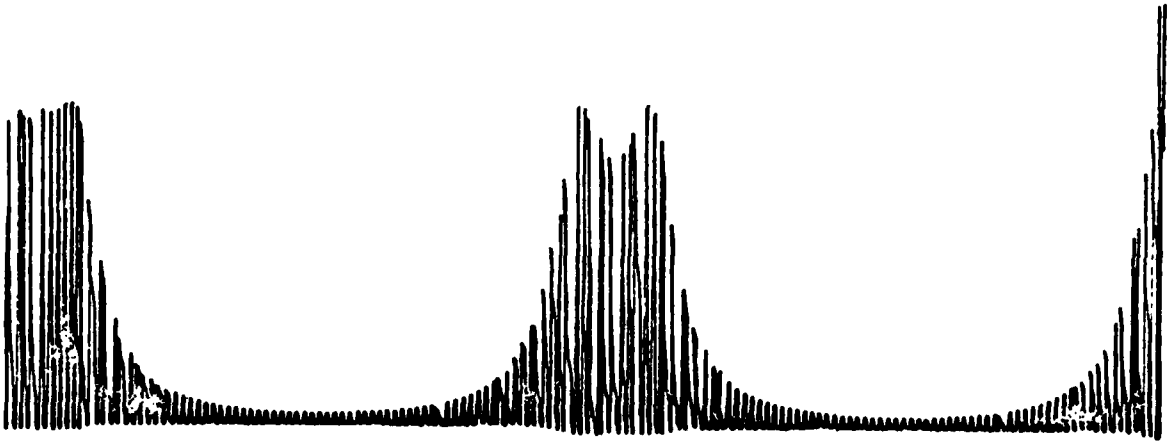

Z VARIATION

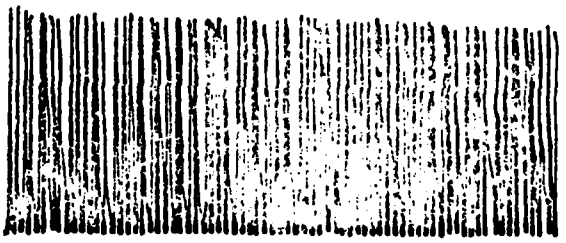

θ VARIATION

FIGURE 8. AXIAL AND AZIMUTHAL VARIATION OF TE_{012} MODE 3030.5 MHZ

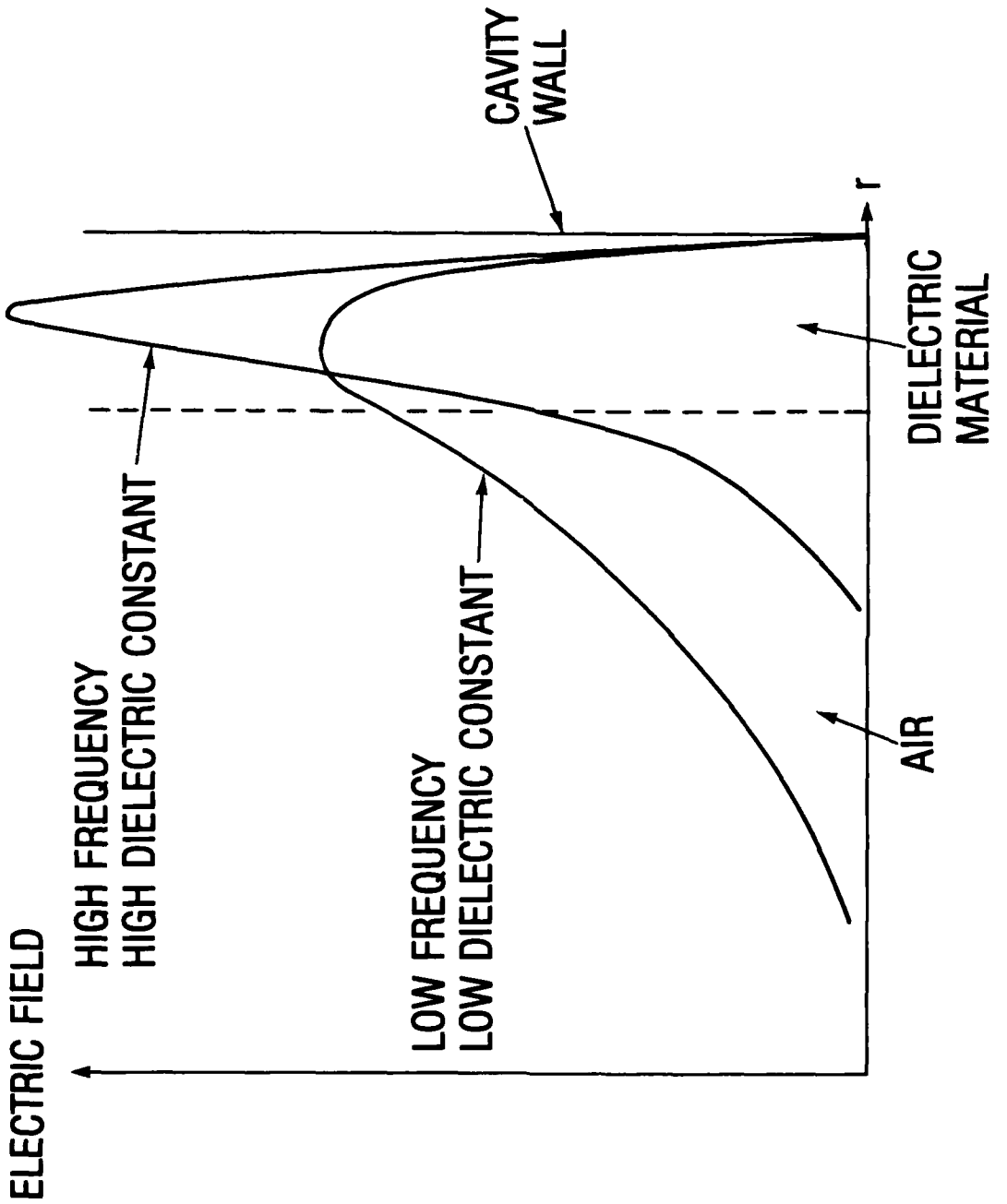

FIGURE 9. EFFECTS OF FREQUENCY AND DIELECTRIC CONSTANT ON PROFILE OF ELECTRIC FIELD IN CAVITY

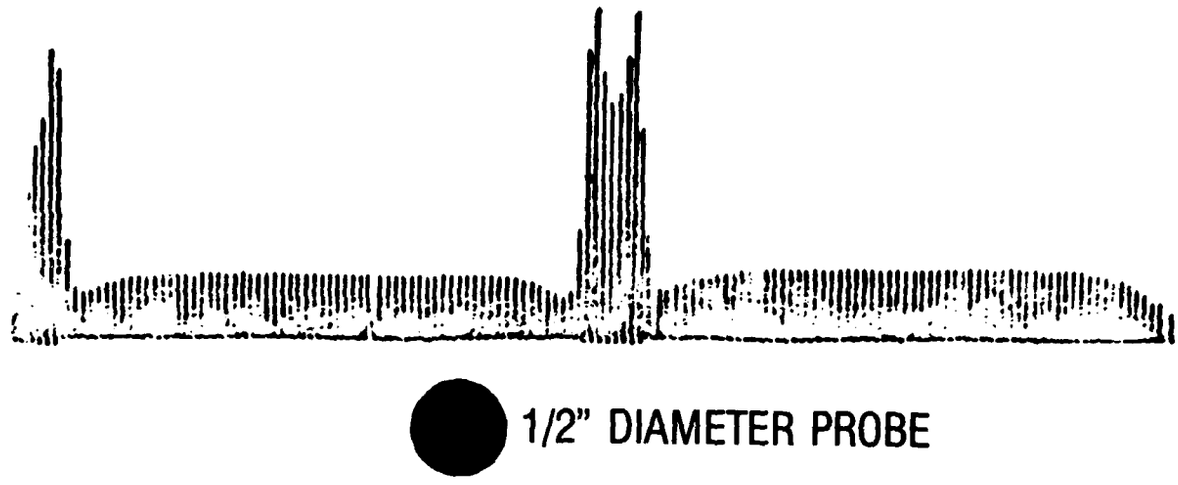

1/2" DIAMETER PROBE

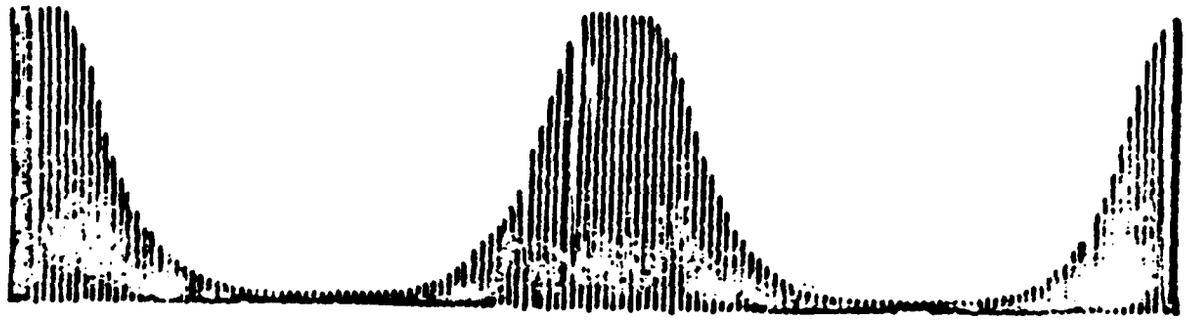

1/4" DIAMETER PROBE

FIGURE 10. EFFECTS OF PROBE SIZE ON AXIAL VARIATION OF TE_{012} EMPTY CAVITY MODE 3087 MHZ

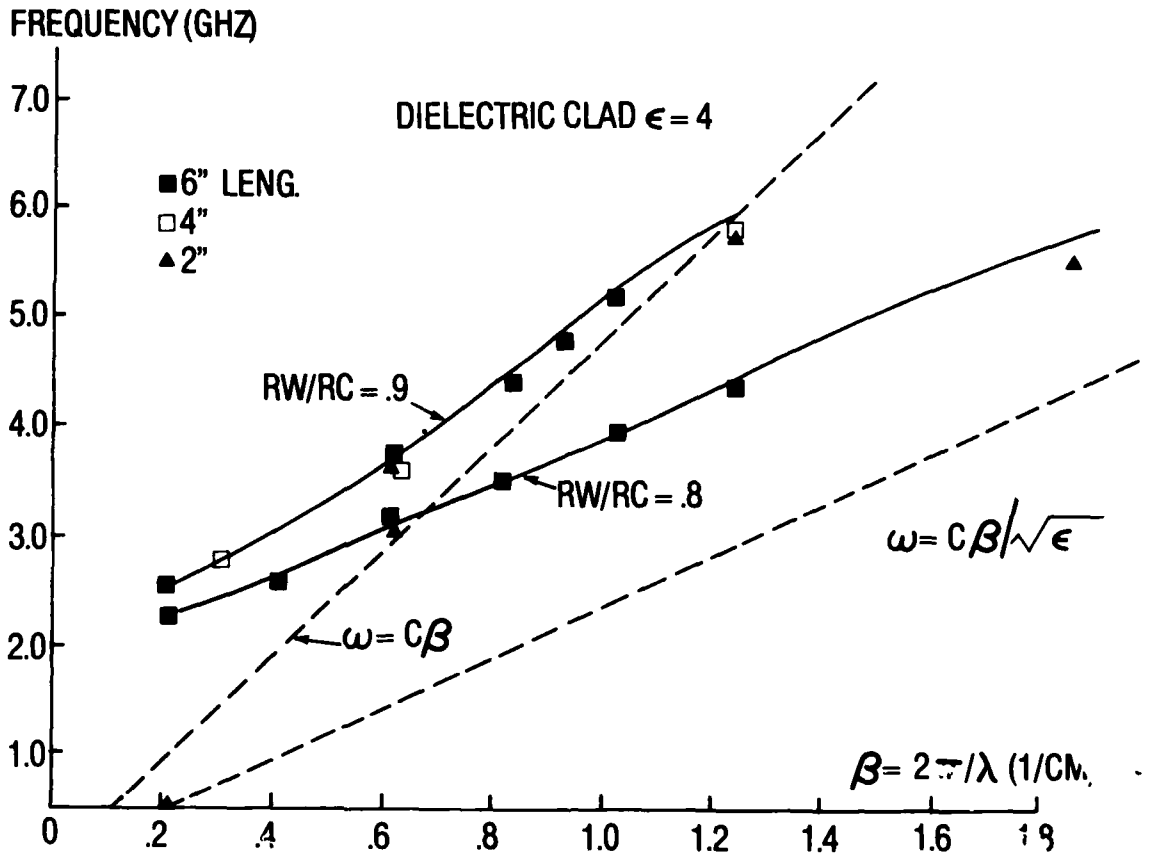

FIGURE 11. DISPERSION CURVES OF DIELECTRIC LOADED CAVITY FOR DIELECTRIC CONSTANT, ε= 4

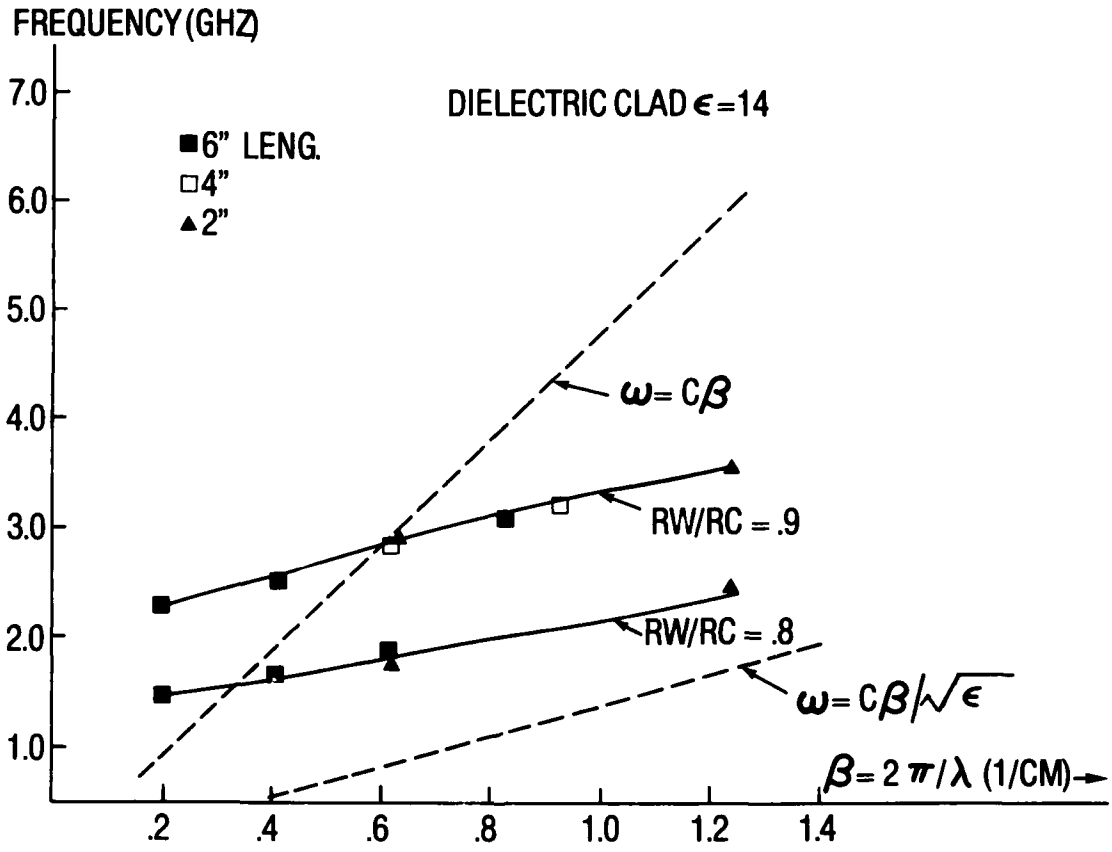

FIGURE 12. DISPERSION CURVES OF DIELECTRIC LOADED CAVITY FOR DIELECTRIC CONSTANT, ε=14

TABLE 1. DATA FOR DIELECTRIC LOADED CAVITY $\varepsilon = 4.0$

6" DIA. CAVITY TEOIN MODES

CAVITY LENGTH	(1/CM) $\beta = 2\pi / \lambda$	N	FREQUENCY (MHZ) RW/RC = .9 THEORY	RW/RC = .9 EXP.	RW/RC = .8 THEORY	RW/RC = .8 EXP.
6"	.2068	1	2543	2521	2248	2253
6"	.4136	2	3041	3030	2629	2590
6"	.6204	3	3718	3690	3094	3123
6"	.8272	4	4478	4435	3557	3516
6"	1.0340	5	5249	5194	4002	3948
6"	1.2408	6			4435	4372
4"	.3102	1	2762	2751		
4"	.6204	2	3718	3364		
4"	.9306	3	4867	4772		
4"	1.2408	4	5947	576		
2"	.6204	1	3718	3620	3094	3029
2"	1.2408	2	5947	5760		
2"	1.8612				5730	5515

TABLE 2. DATA FOR DIELECTRIC LOADED CAVITY ε=14.0

6" DIA. CAVITY TEOIN MODES

			FREQUENCY (MHZ)			
			RW/RC = .9		RW/RC = .8	
CAVITY LENGTH	(1/CM) $\beta = 2\pi / \lambda$	N	THEORY	EXP.	THEORY	EXP.
6"	.2068	1	2285	2270	1461	1421
6"	.4136	2	2602	2563	1625	1656
6"	.6204	3	2912	2912	1821	1820
6"	.8272	4	3165	3123		
4"	.3102	1	2435	2423		
4"	.6204	2	2912	2865		
4"	.9306	3	3280	3212		
2"	.6204	1	2912	2876	1821	1774
2"	1.2408	2	3606	3554	2378	2446

REFERENCES

1. Choe, J.Y., and Uhm, H.S., "Theory of Gyroyron Amplifiers in a Disk or a Helix Loaded Waveguide," Intl. J. Electronics, Vol. 52, 1982, p. 729.

2. Jackson, D., Classical Electrodynamics, (New York: John Wiley & Sons, Inc., 1982), p. 611.

DISTRIBUTION

	Copies
Chief Office of Naval Research Attn: Dr. C.W. Roberson Arlington, VA 22217	1 1
Commander Naval Research Laboratory Attn: Code 6840 (Dr. S. Ahn) Code 6840 (Dr. A.K. Ganguly) Code 6840 (Dr. R. Parker) Code (Dr. Y.Y. Lau) Code (Dr. Pasour) Code (Dr. M.E. Read) Washington, DC 20375	 1 1 1 1 1
Defense Technical Information Center Cameron Station Alexandria, VA 22314	 12
Library of Congress Attn: Gift and Exchange Division Washington, DC 20504	 4
Harry Diamond Laboratory Attn: Dr. H.E. Brandt Dr. A. Bromborsky Dr. A. Kehs 2800 Powder Mill Road Adelphi, MD 20783	 1 1 1
Lawerence Livermore National Laboratory Attn: Dr. B. Kulke (L-436) P.O. Box 808 Livermore, CA 94550	 1
Massachusetts Institute of Technology Attn: Prof. G. Bekefi Bldg. 36-213 77 Massachusetts Ave. Cambridge, MA 02139	 1
Massachusetts Institute of Technology Plasma Fusion Center Attn: Dr. R. Temkin Cambridge, MA 02139	 1
Polytechnic Institute of New York Attn: Dr. S.P. Kuo Route 110 Farmingdale, NY 11735	 1
University of Maryland Electrical Engineering Dept. Attn: Prof. W. Destler Prof. V.L. Granatstein Prof. C.D. Striffler Dr. W. Lawson College Park, MD 20742	 1 1 1 1
University of Maryland Plasma Physics Laboratory Attn: Dr. W.M. Chang College Park, MD 20742	 1
University of Maryland LPFE Attn: Dr. Guillory College Park, MD 20742	 1

DISTRIBUTION (Continued)

	Copies
University California Los Angeles Department of Electrical Engineering Attn: Dr. D.B. McDermott Los Angeles, CA 90024	1
Yale University Mason Laboratory Attn: Prof. J.L. Hershfield 400 Temple St. New Haven, CT 06520	1
Dartmouth College Department of Physics Attn: Dr. J.E. Walsh Hanover, NH 03755	1
Mission Reasearch Corporation Attn: Dr. D. Sullivan 1730 Randolph Rd., SE Albuquerque, NM 87106	1
Pulse Science Attn: Dr. G. Proulx 14796 Wicks Blvd. San Leandro, Ca 94577	1
Science Applications, Inc. Attn: C.L. Chang 1710 Goodridge Dr. McLean, VA 22102	1
Varian Associates Attn: Dr. H. Jory Bldg. 1 611 Hansen Way Palo Alto, CA 94303	1
Raytheon Company Attn: Dr. A. Palevsky Dept. 3671, Code 47 Waltham, MA 02116	1
Raytheon Company Attn: Dr. T. Ruden Code C52-58 Bedford, MA 01730	1

Internal Distribution	Copies
E231	9
E232	3
R41 (J. Smith)	1
R41 (H. Uhm)	1
R43 (J. Cunningham)	1
R43 (J. Choe)	1
R43 (H. Crosby)	10
R43 (D. Jablonski)	1
R43 (A. Krall)	1
R43 (W. Namkung)	1

END

FILMED

12-85

DTIC